

Localization and Source-Strength Estimation of Propeller Cavitation Noise Using Hull-Mounted Pressure Transducers

E.J. Foeth & J. Bosschers (Maritime Research Institute Netherlands)

ABSTRACT

Ships typically have no information on their real-time acoustic underwater signature; the contribution due to cavitation can vary greatly in service conditions and is often worse than as measured at a noise range. A procedure is presented that aims at contributing to an onboard ship-signature estimation procedure detecting cavitation (inception) in the propeller disc. A pressure-transducer array was fitted to both a model-scale (MS) and full-scale (FS) ship; a near-field array processing algorithm was applied to localize the noise source in the propeller disc and to estimate its source level. MS verification tests showed that the array estimated the source location within 10% of the propeller diameter and the source level within 3 dB over most of its frequency range. At full scale a plausible cavitating source location was estimated by the array at low-speed, off-design conditions. A comparison between the source level of the array and as estimated by noise range measurements showed very good agreement within 3 dB up to 16 kHz and within 6 dB up to 40 kHz. At higher ship speeds the loss of coherence of parts of the array—presumably by bubble sweep down over the more outboard transducers—frustrated the source localization. A direct correlation between onboard and noise-range measurements using an assumed source location showed good agreement within 3 dB for straight-ahead sailing conditions.

INTRODUCTION

The underwater radiated noise or acoustic signature of ships is of importance for detection of naval vessels, for sonar self-noise, and for the disturbance it generates for marine mammals and fish, which is also relevant for e.g., fishery research vessels.

The underwater acoustic signature of ships is usually measured at noise ranges. However, the service conditions of the ship may differ from those measured on the noise range. For the propeller the operational condition is influenced by sea state, current, wind, rudder angle and, for controllable pitch propellers, off-design pitch settings. As a result the cavitation inception speed (CIS) and cavitation noise can change

significantly with operational conditions and is nearly always worse than the calm-water conditions at a noise range (van Terwisga et al., 2004).

An onboard system that provides real-time information on the ship signature would be valuable to the ship's crew. An approach for such a system is described by Basten *et al* (2015) where a distinction is made between condition monitoring, condition diagnostics, signature estimation and signature prediction. Condition monitoring is the checking of sensor data for deviations with respect to expected values. If deviations occur then the data is analyzed by the condition diagnostics module to provide possible causes and to suggest interventions. The signature estimation module estimates the signature for the current operational state while the ship signature for a future state, following interventions, is provided by the signature prediction module.

Various methods to determine the acoustic source level (SL) of a cavitating propeller using onboard sensors have been reported in literature. Ten Wolde and De Bruijn (1975) developed an empirical method for the prediction of noise and vibrations onboard the ship by applying the reciprocity principle for the measurement of the acoustical source strength of cavitating propellers. The transfer function between a linear electro-mechanical or electro-acoustical transducer and the propeller disc was determined by using the transducer as an actuator and measuring the resulting pressure with a hydrophone at selected positions in the propeller disc. Results for seven ships were reported by de Bruijn et al (1986). Basten et al (2015) applied accelerometers to estimate the ship acoustic signature using transfer functions between hull and two examples of the relation between onboard measured noise using a hull-penetrating hydrophone and offboard measured underwater noise. The onboard measurements were corrected for the solid boundary factor of the ship hull and spherical spreading loss; the offboard measurements were only corrected for spherical spreading loss. The results showed very good agreement above 250 Hz for one ship and above 1 kHz for another ship. At lower frequencies it was observed that the offboard measured levels were smaller than the onboard

measured levels; this was most likely due to the influence of the free surface on the offboard measured levels (Lloyd mirror effect). The acoustic source strength at the first few blade rate frequencies was determined by van Wijngaarden (2011) by using a few hull-mounted pressure transducers. The source strength and the position of an acoustic monopole was determined using an acoustic boundary element that solves for the scattering effect of the hull. The same methodology was used by Lee et al (2014).

These results imply that specific transfer-function measurements are not required if pressure sensors or hydrophones are used as onboard sensors. The acoustic source strength is sensitive to the position of the cavitation when the sensor is near and this position is difficult to estimate if only a few sensors are used and when only low-frequency data is used. The location of cavitation can be found by array processing of hydrophone data for which several techniques are available: time difference of arrival, Lee et al (2012), beam forming, Abbott et al (1993), Park et al (2016), matched field processing, Park et al (2009), Kim et al (2015) and ray propagation combined with Monte Carlo technique, Chang and Dowling (2009). A description of source localization techniques for other applications is given in e.g., Brandstein & Ward (2001).

This paper presents a methodology and results for the estimation of the acoustic source strength of a cavitating propeller by using a sparse array of hull-mounted pressure transducers above one propeller of a twin-screw vessel. The methodology includes localization of the acoustic source by applying near-field beam forming. We present the derivation of the near-field algorithm verified by test results at model scale using a sound projector in the propeller disc, and validated with a model scale experiment with a cavitating propeller. Next, results of the array at full scale are presented including a discussion on the performance of the array and difficulties encountered thus far. Results are shown for a vessel with a cavitating propeller including a comparison with noise range data. We assume here that the collapse of the cavitation is a compact noise source that can be represented by a single, stationary monopole in a quiescent fluid; the acoustic source can be considered stationary in location as the cavitation collapse usually recurs in the same location in the propeller disc. For well-developed cavitation the validity of the assumption of compactness may no longer apply depending on the cavitation extent and appearance of cavitation at other locations. The type of cavitation (e.g., sheet or tip vortex, suction or pressure side) can only be inferred from the estimated source location.

NEAR-FIELD BEAM FORMING

In this section we present the array processing procedure applied to both model and full scale experiments. As our cavitating noise source is located within the array aperture we use a near-field formulation, that is, we must assume spherical wave spreading from the source to the array and cannot use the planar-wave assumption of a far-field array.

We assume that the sensors register the noise from the source directly and do not take the effect of noise scattering by the hull appendages into account. For an array with M sensors, the pressure of the source $S(t)$ with amplitude $|S|$ at a frequency ω as registered by sensor i results in a signal x^i

$$x^i(\omega) = S \frac{e^{-ikR_s^i}}{R_s^i} + N = \frac{|S| e^{-i(\omega + kR_s^i)}}{R_s^i} + N \quad (1)$$

with k the wave number, R_s^i the distance between the source and sensor i and N the contribution of noise. We recognize the propagation vector d with the spherical attenuation and phase delay

$$d^i(\omega) \equiv \frac{e^{-ikR_s^i}}{R_s^i} \quad (2)$$

For the far-field formulation the attenuation difference between sensors is negligibly small and the attenuation term $1/R_s^i$ is typically dropped from expression of the propagation vector. For the remainder we drop the term ω from the notation. Our main goal concerns incipient cavitation and therefore the assumption of a single noise source is sufficient for now. Christensen & Hald (2004) formulated a method termed Cross-Spectral Imaging (CSI). If a source location in the flow is selected then under ideal circumstances the *expected* cross-spectrum between sensors (m, n) —without noise—is equal to

$$\phi_{ee}(m, n) = |E|^2 d_e^m \overline{d_e^n} \equiv |E|^2 \Gamma_{ee}(m, n) \quad (3)$$

whereby E is the (unknown) expected amplitude and $\Gamma_{ee} = d_e d_e^H$ the so-called steering-vector correlation matrix¹ that is a function of frequency and distance only. We can determine the difference between the

¹ $A^H = \overline{A}^T$, Hermitian, or, complex conjugate transpose

expected correlations $\phi_{ee} = |E|^2 \Gamma_{ee}$ with the measured correlation ϕ_{xx} , and obtain an error function

$$\varepsilon(e) = \frac{1}{M^2} \sum_{n=1}^M \sum_{m=1}^M \left| \phi_{xx} - |E|^2 \Gamma_{ee} \right|^2 \quad (4)$$

We minimize the error ε by applying a least-squares approach to obtain the best fit for $|E|$, or²

$$|E| \approx \sqrt{\frac{\Gamma_{ee}^H : \phi_{xx}}{\Gamma_{ee}^H : \Gamma_{ee}}} \quad (5)$$

Now³

$$\begin{aligned} |\phi_{xx} - \phi_{ee}|^2 &= \phi_{xx} : \phi_{xx}^H - |E|^2 (\phi_{xx}^H : \Gamma_{ee}) \\ &\quad - |E|^2 (\phi_{xx} : \Gamma_{ee}^H) + |E|^4 (\Gamma_{ee}^H : \Gamma_{ee}^H) \end{aligned} \quad (6)$$

Substitution of (5) into (4) and as both Γ_{ee} and ϕ_{xx} are self-adjoint⁴, $\phi_{xx}^H : \Gamma_{ee} = \phi_{xx} : \Gamma_{ee}^H = \phi_{xx} : \Gamma_{ee}$

$$|\phi_{xx} - \phi_{ee}|^2 = \phi_{xx} : \phi_{xx}^H - \underbrace{\frac{(\Gamma_{ee} : \phi_{xx})^2}{\Gamma_{ee} : \Gamma_{ee}}}_{IF^2} \quad (7)$$

As the first term depends on the measurement only, minimization of this error, that is a function of the source position, equals maximization of the second term in the right-hand side (RHS). We can find our most probable source location by scanning points in the flow domain and search for the maximum value of the second term. This term is referred to as the Imaging Function IF (squared) by Christensen & Hald. For the nominator and denominator of the IF we notice the following relations⁵

$$^2 A : A = \sum_{i=1}^M \sum_{j=1}^N A_{ij} B_{ij} = tr(A^T B) = tr(AB^T)$$

³

$$|\phi_1 + \phi_2|^2 = (\phi_1 + \phi_2)(\phi_1 + \phi_2)^H = \phi_1 \phi_1^H + \phi_1 \phi_2^H + \phi_1^H \phi_2 + \phi_2 \phi_2^H$$

$$^4 A = A^H$$

⁵ If $A = aa^H$, $B = bb^H$ then

$$\begin{aligned} A : B &= tr(AB^T) = tr(aa^H (bb^H)^T) = tr(aa^H \bar{b}b^T) \\ &= a^H \bar{b} tr(ab^T) = a^H \bar{b} a^T b = a^H \bar{b} a^H \bar{b} = |a^H \bar{b}|^2 \end{aligned}$$

$$\begin{aligned} (\Gamma_{ee} : \phi_{xx})^2 &= |d_e^H x|^4 = (d_e^H \Gamma_{xx} d_e)^2 \\ \Gamma_{ee} : \Gamma_{ee} &= (d_e^H d_e)^2 \\ d_e^H d_e &= \sum_{i=1}^M \left(\frac{1}{R_e^i} \right)^2 \end{aligned} \quad (8)$$

We can write the IF and amplitude estimate in terms of the propagation vector and signals

$$\begin{aligned} IF &= \frac{|d_e^H x|^2}{d_e^H d_e} = \frac{d_e^H \Gamma_{xx} d_e}{d_e^H d_e} \\ |E| &= \sqrt{\frac{|d_e^H x|^2}{(d_e^H d_e)^2}} = \sqrt{\frac{d_e^H \Gamma_{xx} d_e}{(d_e^H d_e)^2}} \end{aligned} \quad (9)$$

where we write $|d_e^H x|^2 = d_e^H \Gamma_{xx} d_e$, so that we can use average cross-power spectral density in order to reduce the influence of uncorrelated noise. When the distance between source and sensors on the array is identical for all sensors, the near-field imaging function reduces to the far-field formulation whereby d contains phase information only and $d_e^H d_e = M$. In the imaging function we recognize the array output

$$O = \sqrt{IF} = \frac{d^H x}{\sqrt{d^H d}} \quad (10)$$

NEAR-FIELD MVDR

The second procedure that has been investigated is the (far-field) Minimum Variation Distortionless Response (MVDR) method of Frost (1972), also referred to as super directivity, that we here derive for the near-field formulation. Noise or interference from other directions than the interrogation direction is preferably removed; sensor shading is applied whereby a phase and amplitude correction is applied and the propagation vector d is replaced by a steering vector w . The array output squared $w^H \Gamma_{xx} w$ is minimized with respect to the contribution of noise and the steering vector maximizes the output for the direction of view, or, $d^H w = c$; for the far-field formulation $c = 1$. The values for w follow from a constrained minimization by using Lagrangian multipliers Λ

$$\begin{aligned} F &= w^H \Gamma_{NN} w + \Lambda (d^H w - c) \\ \frac{\partial F}{\partial w} &= 0, \frac{\partial F}{\partial \Lambda} = 0 \end{aligned} \quad (11)$$

If $\partial F/\partial w = 0$ then $\overline{\partial F/\partial w} = 0$ it follows⁶ that

$$\overline{\frac{\partial F}{\partial w}} = \Gamma_{NN}^T w + \Lambda d = 0 \quad (12)$$

$$\overline{\frac{\partial F}{\partial \Lambda}} = d^H w - c = 0 \quad (13)$$

From eq. (12) it follows $w = -\Lambda \Gamma_{NN}^{-1} d$, substitution in eq. (13) leads to $\Lambda = -c(d^H \Gamma_{NN}^{-1} d)^{-1}$ so that

$$w = \frac{c \Gamma_{NN}^{-1} d}{d^H \Gamma_{NN}^{-1} d} \quad (14)$$

Now, for our near-field formulation we take the attenuation by spherical spreading into consideration and write $c = \sqrt{d^H d}$ to obtain

$$w = \sqrt{d^H d} \frac{\Gamma_{NN}^{-1} d}{d^H \Gamma_{NN}^{-1} d} \quad (15)$$

and our array output is now equal to

$$O = w^H x = \sqrt{d^H d} \frac{(\Gamma_{NN}^{-1} d)^H x}{d^H \Gamma_{NN}^{-1} d} \quad (16)$$

The array's ability to suppress noise can be estimated by assuming a homogenous diffuse noise field (e.g., Brandstein & Ward, 2001) of which the noise-correlation matrix is given by

$$\Gamma_{NN}^{m,n} = \text{sinc}\left(\frac{k}{2\pi} |R_s^m - R_s^n|\right) \quad (17)$$

At the lower frequencies $k \rightarrow 0$ and $\lim_{x \rightarrow 0} \text{sinc } x = 1$ so Γ_{nn}^{-1} becomes increasingly more ill-posed. Following Bitzer & Simmer (2001), one can redefine the noise correlation matrix by dividing the non-diagonal elements with a user-defined parameter $1 + \mu$, thereby artificially reducing the cross-correlated noise. If $\mu \rightarrow \infty$, or, when no noise is present at all, then $\Gamma_{NN} = I$ and for the array output squared we

⁶ Recall the Wirtinger derivatives, $\frac{\partial}{\partial w} d^H w = \bar{d}$,

$\frac{\partial}{\partial w} w^H \Gamma_{xx} w = (w^H \Gamma_{xx})^T = \Gamma_{xx}^T \bar{w}$ and $\Gamma_{xx}^T = \bar{\Gamma}_{xx}$

obtain the imaging function of Christensen & Hald in eq. (9), that appears a variation of the more general, near-field MVDR formulation. Here we reserve the term CSI for $\mu \rightarrow \infty$. Note that $\Gamma_{NN} \approx I$ when the wave length becomes of similar size as the sensor spacing which is near the design frequency of the array, even when $\mu = 0$, and the difference between the MVDR and CSI becomes vanishingly small and is only apparent at lower frequencies. For our imaging function we can now write

$$IF = \frac{w^H \Gamma_{xx} w}{w^H w} \quad (18)$$

For Γ_{xx} we use the average cross-power spectral density computed from 66% overlapping time series on which a Hanning window is applied. The imaging function we present are given in one-third-octave (OTO) bands for further averaging. The values are normalized with the maximum value, converted to a logarithmic scale and plotted as iso-contours from -12 to 0 dB. The SLs were corrected for the solid boundary factor for which a factor 2.0 is assumed, corresponding to a pressure doubling at the hull.

When using no or predetermined noise-correlation matrices, the expression for w only depends on the frequency, position of the sensors and source locations under consideration and can be pre-calculated for a fixed interrogation domain, such as a region encompassing the propeller location. Using a noise correlation matrix as measured was not yet attempted for reasons outlined below in the section on turbulent boundary layer pressure fluctuations.

MODEL SCALE TEST SETUP

The array processing methods have been tested at model scale using a twin-screw ship model of length 7.9 m between perpendiculars. The tests were focused on localization of cavitation in the propeller plane and a beam-wise array consisting of nine PCB112A22 pressure transducers (PTs) with constant spacing of $l = 48.8$ mm (design frequency 15 kHz) was fitted above the port-side propeller, resulting in an array aperture of about 130% of the propeller diameter. All PTs were fitted in a 260x460x50mm Perspex block to allow illumination of the ship propeller from within the ship model and to reduce the influence of vibrations. PCB M607A11 accelerometers were fitted to both the Perspex block and the ship model made of wood. All transducer data was sampled at 96 kHz.

The tests were performed in the Depressurized Wave Basin (DWB) using its silent towing carriage

developed for the measurement of propeller cavitation noise, (Bosschers et al. 2013). The DWB was fitted with two hydrophones (RESON TC4014) fixed on a mast positioned in the middle of the basin with the ship model sailing over the mast. The keel-aspect hydrophone was positioned on the center line of the basin at a depth of 1.5 m and the beam-aspect hydrophone was positioned at a distance of 2.2 m from the center line to port at a depth of 1.1 m. The minimum distance from keel and beam hydrophone to propeller tip was 1.4 and 2.2 m, respectively. The sample rate of the hydrophones was 300 kHz. The cavitation noise measurement procedure in the DWB and comparison between model and full scale results is described by van der Kooij & de Bruijn (1984) and Lafeber & Bosschers (2016). The influence of reverberation including the effect of the free-surface on the noise measurements (Lloyd mirror effect) is discussed by Lafeber et al (2015).

MODEL SCALE VERIFICATION SETUP AND RESULTS

Sound projectors have been positioned at different, known positions in the propeller disc to verify the array processing methods. Bruel & Kjaer hydrophones BK8100 and BK8103 driven by a Bruel & Kjaer power amplifier 2713 were used as sound projectors in combination with an AGILENT signal generator. Exponential sine sweep of 0.5 s from 5 kHz to 35 kHz were generated. The minimum distance to a wall was 8 m (tank bottom) resulting in a reflection with a delay of about 11 ms. The sine sweeps were repeated for at least 30 seconds to capture a minimum of 60 sweeps. The sound-projector tests were all performed in atmospheric conditions, zero carriage speed and positioned such that the center of the propeller was at the same longitudinal position in the tank as the hydrophones. The dissolved gas content during the measurements was 27% of the saturation level, measured at atmospheric pressure.

The BK8100 hydrophone was fitted to the pitot-tube traversing system normally used for wake field measurement equipment—Figure 1—the propeller was not present during these tests. The sound-source position could be easily moved through the propeller disc both radially and tangentially. Selected radial positions were at 0.35, 0.70 and 1.00 times the propeller tip radius R_p . Each radial position was measured at eight angular positions spaced out equally, starting in the top position (12 o'clock), resulting in a source-to-sensor distance ranging from 68 to 209mm with the source in the top position at $1.0R_p$.



Figure 1: Aft shaft bracket and the wakefield measurement equipment fitted with a hydrophone and the perspex block with the pressure transducers forming the array.

When the source was located in the top position its location was found accurately. At the lower position of the disc, with the source roughly one array aperture distance below the array, the accuracy of the source position becomes less as the position is in the transition region between near and far field; the depth perception of the array is reduced but the direction is well captured.

In Figure 2 a typical result of an IF is shown, here for frequencies of 15, 17.5, 20 and 22.5 kHz with the source at $1.0R_p$ and rotated 45 degrees over the top (as indicated by the red dot). All IFs are presented for the face-view, port-side propeller. If we take the -1dB line as an uncertainty limit the source location has an uncertainty of about $0.2R_p$ in array depth and with a good angular confinement. Note that these frequencies exceed the far-field aliasing criterion ($l < \frac{1}{2}\lambda$) that would normally limit the array to about 15 kHz; mild aliasing was observed to develop for 22.5 kHz.

Figure 3 shows the summed IFs in an OTO band of 16 kHz without (CIS, A) and with (MVDR, $\mu=1$, B) noise suppression; both results clearly indicate in what region of the propeller disc the source is present, and MVDR expectedly results in a minor reduction in the location uncertainty. Although the White-Noise Gain $G_{WN} \equiv |w^H d|^2 / w^H w$ degrades simultaneously one can combine the location estimation from MVDR with the source level estimate from CSI.

The spectrum of the SL for the source at $1.0R_p$, 6 o'clock position, as estimated by the array using eq. (9) for the position as estimated using the array results for an OTO band with center frequency of 10 kHz is presented in Figure 4, also presenting the SL as emitted by the source and as measured by two tank hydrophones (corrected for distance and free-surface effect) for the sound projector in the 6 o'clock position, respectively. Up to 15 kHz the level was well captured within 3 dB but above 15 kHz larger differences were observed, possibly due to reflection by the shaft, struts and traversing mechanism. Below 5 kHz the SL was due to background noise. The SNR of the pressure transducers and tank hydrophones within the sweep frequency range was above 12 dB and 25 dB, respectively. The correlation with the tank hydrophones was good up to 15 kHz, above 15 kHz a difference of 3 dB was obtained.

It is observed that the estimate of the source strength by the array and the tank hydrophones was in good agreement between 5 and 30 kHz except around 20 kHz, requiring further investigation. The oscillatory character of the levels predicted by the tank-based hydrophones was due to interference patterns by free surface reflections was very clearly present in the narrow band spectra (not shown here). As the model was not moving, no free-surface waves were generated and the free surface remained a near-perfect mirror; with a sailing model no free surface interference pattern was observed in the frequency range presented here.

The BK8100 and BK8103 hydrophones were also mounted on the propeller to investigate the scattering effect of the propeller on the measurements. When the source was located in the upper half of the propeller disc—Figure 5A—the estimated location was weakly affected by the presence of the propeller. The spectrum of the SL presented in Figure 6A shows a considerable influence below 10 kHz, however, the correlation with the hydrophones in the tank remained good. When the source is in the 6 o'clock position the location was not recovered well—Figure 5B—and the SL estimation immediately degraded, see Figure 6B. Although the recovery of a source in the lower half of the propeller disc is likely not required for the current vessel, these results do emphasize the importance of a correct estimation of the source location and is identified as a risk of a near-field array; a difference of one propeller diameter in the position can cause a difference of 8 dB in the source levels.

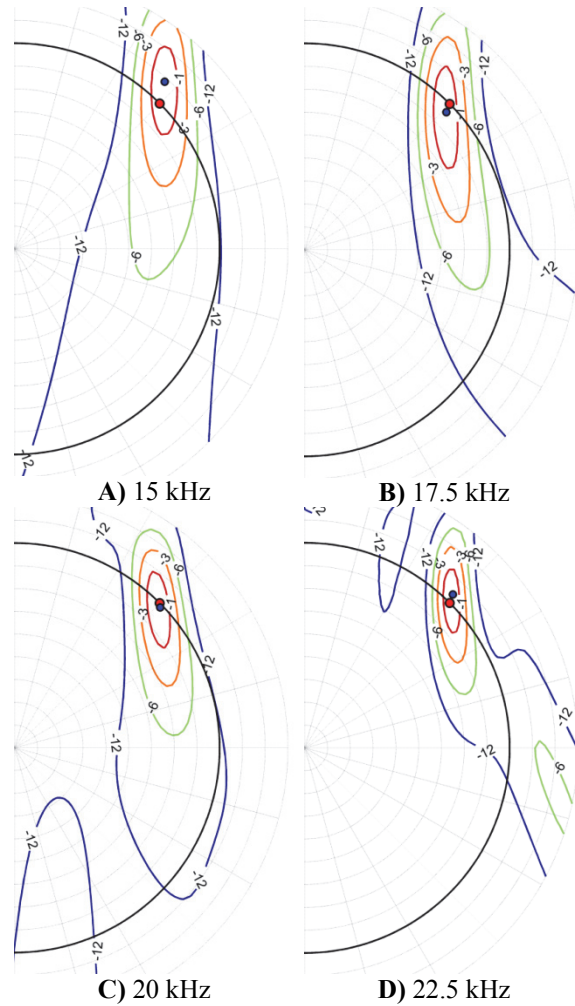


Figure 2: Imaging function from CSI for the source at $1.0R_p$ and 45 degrees position for different frequencies, no noise correlation.

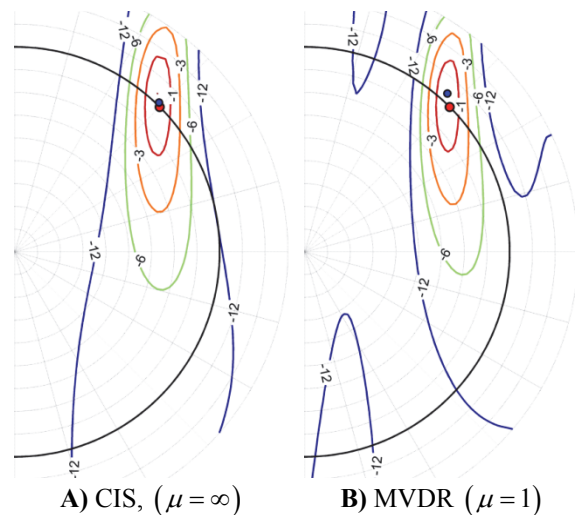


Figure 3: Imaging Functions of the 16 kHz OTO band, source position as in Figure 2.

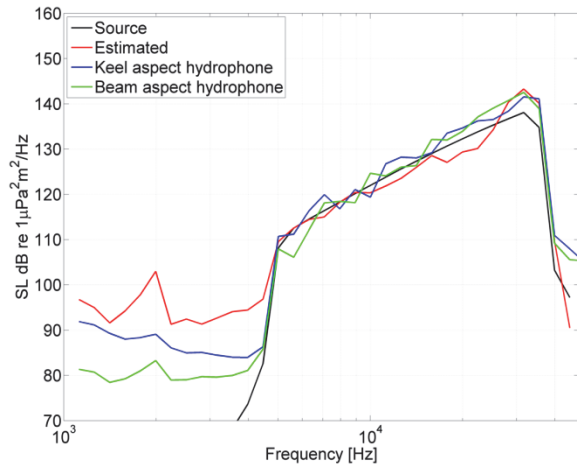


Figure 4: SL in 1/6th octave bands as estimated by the array and the tank hydrophones compared to as emitted by the source at the bottom of the propeller disc position.

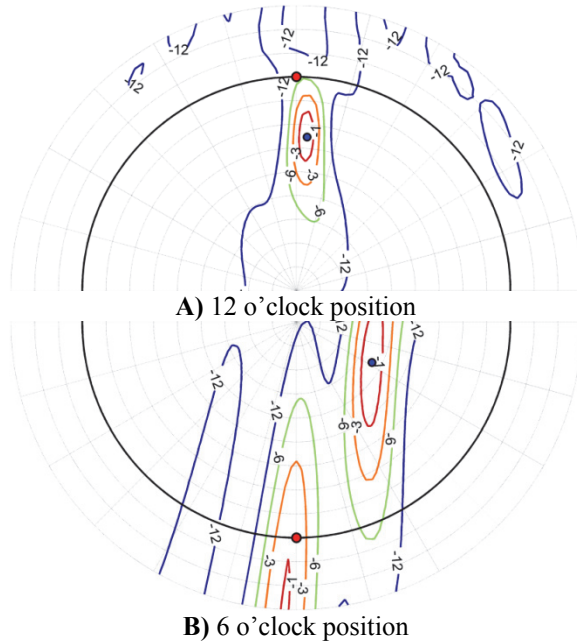
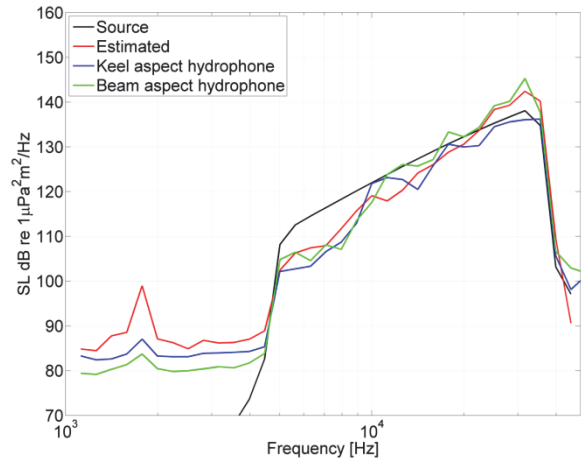
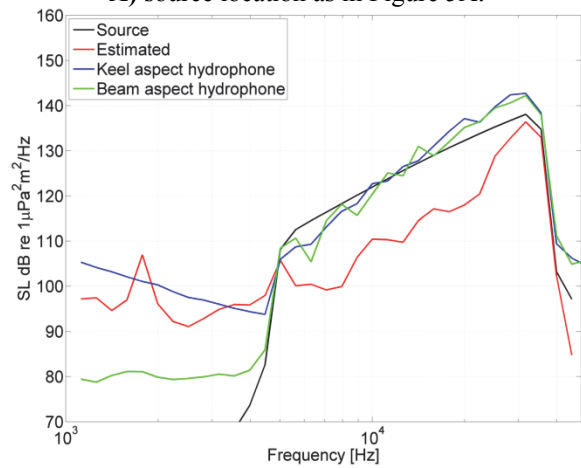


Figure 5: Imaging function from CSI for an OTO band with a center frequency 10 kHz. for the source fixed to a model propeller blade at $0.7R_p$ with the actual (red) and estimated (blue) location outlined.



A) source location as in Figure 5A.



B) source location as in Figure 5B.

Figure 6: SL in 1/6th octave bands as estimated by the array and the tank hydrophones compared to as emitted by the source (attached to propeller).

CAVITATION TEST RESULTS

A series of measurements were performed with a cavitating propeller (only the port side propeller was fitted). One example is shown at high ship speed where sheet cavitation at the tip of the propeller and some blade root cavitation was present, see Figure 7A. The submerged side illumination equipment normally used during the cavitation tests was not present resulting in an underexposure. The results of the source localization in Figure 7B,C show acceptable agreement with the observations.

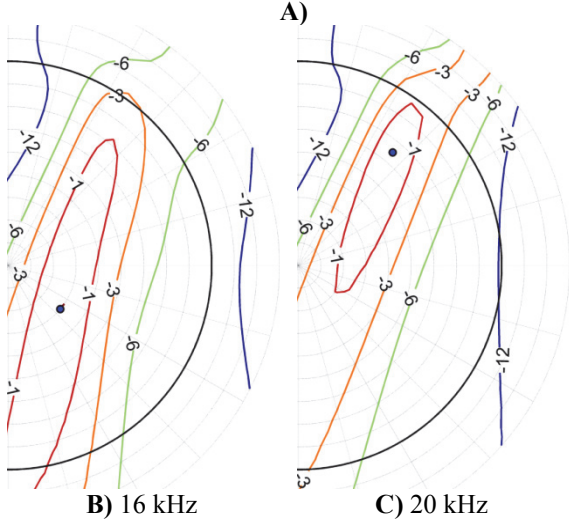


Figure 7: High speed video frame showing cavitation on the propeller (A) and corresponding IFs for two OTO bands. As all IFs are presented as a face-view, the suction-side image of the propeller has been mirrored horizontally.

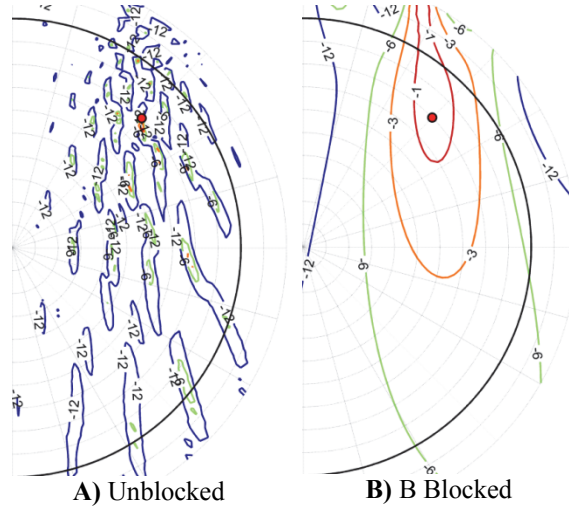


Figure 8: Results of the array processing using a simulated source and a sparse array showing the effect of the blocking matrix for 5 sub arrays spaced equally over one propeller diameter in a horizontal plane above the propeller tip with 3 sensors each.

FULL-SCALE TEST SETUP

The model-scale array aperture is preferable scaled geometrically but the design frequency of the array is not: for the full-scale design of the array the main frequency of interest was selected at 10 kHz for reasons of maximum expected SNR in combination with the selected transducer. This resulted in a full-scale sensor spacing of 75 mm. As the number of sensors for full scale needed to remain small for practical reasons and the array aperture must remain as wide as possible to remain in the near-field formulation, a sparse array was applied whereby groups of sensors were placed only locally meeting the aliasing criterion. As such, we obtain a sparse array of sub-arrays.

Testing with simulated sources for a sparse array approximating the dimensions of the full scale setup shows that strong aliasing occur, see Figure 8A. These aliasing regions shift with frequency and may cancel out when summed in OTO bands, but such an approach may lead to spurious results. Instead, a blocking matrix B was applied to our signal correlation matrix⁷

$$\Gamma_{ww} = B \circ (dd^H)$$

$$B_{ij} = \begin{cases} 1 & |p_i - p_j| \leq L \\ 0 & \text{otherwise} \end{cases} \quad (19)$$

with p_i the location of sensor i , and L the aperture of each sub array; the results as in Figure 8B were obtained. The aliasing was reduced at the cost of a much larger uncertainty of the source location estimation but the uncertainty was in the same order as the model test approach clearly indicating a source location in the propeller disc. The application of the blocking matrix had the additional advantage that only the spacing between sensors in each sub array needs to be known accurately while the uncertainty in spacing between the sub arrays themselves could be much larger. This was of great benefit as placement of the sensors onboard had to be performed with the ship along the quay—not in dry dock—with no opportunity to accurately measure the transducers position from the outside. The sensor position within each sub-array could be measured accurately from the inside of the ship while the positions of the sub arrays had to be obtained from distances to e.g., bulkheads and stiffeners. Simulations showed that the expected uncertainty of 10-30 mm in sub-array position did not contribute to the overall uncertainty of the array

⁷ $(A \circ B)_{i,j} = A_{i,j}B_{i,j}$, Hadamard product.

processing. With a limited number of sensors available it was decided to apply four sub arrays with three transducers each with a total array aperture spanning 72.5% of the propeller diameter, focusing mainly on the down-going blade where cavitation inception was known to occur from previous (visual) observations. The array layout is shown in Figure 9A.

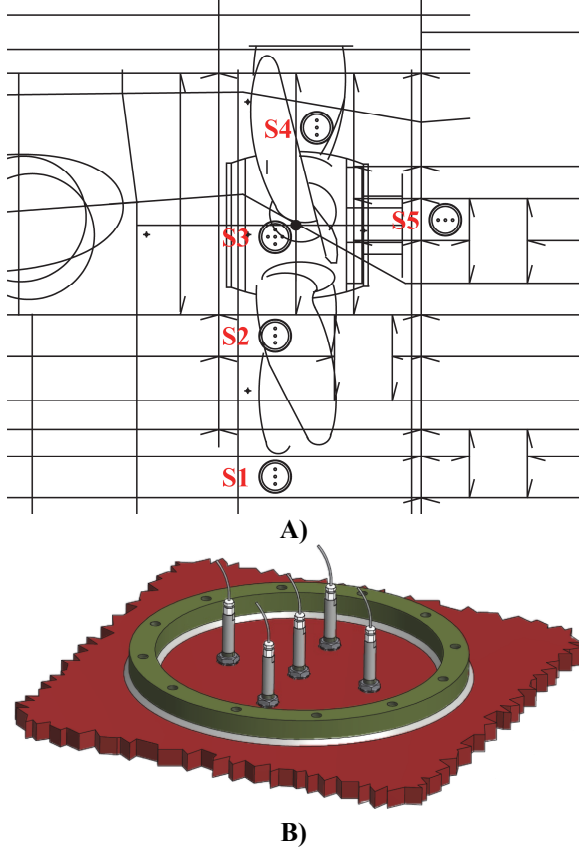


Figure 9: A: Layout of the array above the port side propeller, rudder at left showing the location of sub arrays S1 to S5. B: Rendering of a sub array S3 comprised of a steel ring with an outer diameter of 330 mm and 5 transducers.

Each sub array was designed as a steel ring of 33 cm diameter welded to the hull to offer stiffness after drilling through the shell; within this ring a row of transducers was fitted with a sensor spacing of 75 mm. After the experiments the transducers were removed, replaced by a bolt and a watertight flange was fitted. Figure 9B shows that sub array 3 has two additional sensors to check the location of the source in lengthwise direction. The signals of the transducers were acquired at 96 kHz, with an anti-aliasing filter in the acquisition system this resulted in a maximum useable frequency of 40 kHz.

A high-speed video camera observing the propeller was placed at previously installed observation windows. However, weather conditions and illumination were generally bad and bubble sweep down at higher speeds resulted in no useable (high-speed) footage of the propeller for visual confirmation of the cavitation on the propeller. Information of the cavitation behavior of the propeller was therefore only available from previous trials and from model scale tests. The noise of the ship was measured at a noise range and is presented for a beam hydrophone positioned at 30 m depth and 100 m distance from the track.

TURBULENT BOUNDARY LAYER PRESSURE FLUCTUATIONS

We compare the measured background noise spectra, obtained from non-cavitating conditions to spectra of the turbulent boundary layer pressure fluctuations (TBLPF) following Goody (2004) and Goody et al. (2007), who showed that the TBLPF spectrum of a ship model hull is consistent with the TBLPF spectrum of a flat plate. In their approach, the local wall shear stress τ_w was estimated using the Prandtl-Schlichting relation for a turbulent boundary layer at ship speed V_s

$$\tau_w = \left(\frac{1}{2}\rho V_s^2\right) 0.427 (\log \text{Re} - 0.407)^{2.64} \quad (20)$$

with the Reynolds number Re here defined as

$$\text{Re} = 0.95 \frac{V_s L_{pp}}{\nu} \quad (21)$$

with L_{pp} the ship length between perpendiculars and ν the kinematic viscosity. The friction velocity is then estimated by

$$u_\tau = \sqrt{\frac{\tau_w}{\rho}} = 0.4621 V_s (\log \text{Re} - 0.407)^{1.32} \quad (22)$$

Goody's relation for the power spectral density $\Phi(\omega)$ is given as

$$\frac{\Phi(\omega) V_s}{\tau_w^2 \delta} = \frac{3.0 \left(\frac{\omega \delta}{V_s}\right)^2}{\left[\left(\frac{\omega \delta}{V_s}\right)^{0.75} + 0.5\right]^{3.7} + \left[1.1 R_T^{-0.57} \left(\frac{\omega \delta}{V_s}\right)\right]^7} \quad (23)$$

with δ the local turbulent boundary layer thickness estimated from plate theory using $\delta = 0.37L \text{Re}^{-\frac{1}{2}}$ and with R_T the time-scale ratio to distinguish between the contributions of the inner and outer boundary layer represented in eq. (23)

$$R_T = \frac{u_\tau \delta}{\nu} \sqrt{\frac{C_f}{2}} = \frac{\delta}{\nu} \sqrt{\frac{\tau_w C_f}{2\rho}} = \frac{\delta V C_f}{2\nu} \quad (24)$$

The local friction coefficient is estimated by

$$C_f = 0.045 \text{Re}^{-\frac{1}{4}} \quad (25)$$

We here multiply the RHS of eq. (23) by 2π as $\overline{p^2} = 2 \int_0^\infty \Phi(\omega) d\omega = 4\pi \int_0^\infty \Phi(2\pi f) df$, rearrange and we obtain the PSD of the TBLPF in terms of frequency

$$\Phi(f) = \frac{3\tau_w^2 f^2 \left(\frac{2\pi\delta}{V_s}\right)^3}{\left[\left(\frac{2\pi f \delta}{V_s}\right)^{0.75} + 0.5\right]^{3.7} + \left[1.1R_T^{-0.57} \left(\frac{2\pi f \delta}{V_s}\right)\right]^7} \quad (26)$$

A comparison between the estimation of the TBL thickness and local friction coefficient from flat plates and the results from a RANS calculation (not presented) showed that the boundary layer thickness at the transducers in the stern region is underestimated by a factor of 2 to 3 and that the friction coefficient agrees to within 20%, however, the effect on Goody's spectral estimate is small (<3 dB) and the flat plate assumption was sufficiently accurate for our purposes. The same holds for using the ship speed for the velocity at the edge of the boundary layer at the transducer position.

The TBLPF are caused by turbulent structures advected by the bulk flow and the orientation of these structures in the flow determine the (spatial) wave-number spectrum; the net pressure force on the sensor surface will go to zero when the spatial wave length is much smaller than the sensor diameter and the wave spectrum as measured depends on the sensor size that effectively acts a low-pass filter. A correction of the spectrum for the sensor size has been proposed by Corcos (1963), given as

$$\frac{\Phi_{\text{measured}}}{\Phi} = f\left(\frac{\omega r}{U_c}\right) \quad (27)$$

whereby U_c is the advection velocity of the pressure fluctuations in the TBL, itself a function of the frequency and TBL displacement thickness. The ratio between U_c and velocity at the edge of the boundary layer is reported as a factor between 0.61 and 0.76 and was taken as 0.61 for convenience. The effective sensor radius is taken as half the total surface diameter of the sensor.

An example of the power spectral density of some of the transducers at ship speed below the CIS is shown in Figure 10 with Goody's spectral estimate including Corcos' correction. From the figure it is plausible the measurements below 1 kHz (at the reported speed) were due to TBLPF only. The frequency range where TBLPF was measured increased with ship speed up to 5-6 kHz. For the cavitating ship speeds that were analyzed, the cavitation noise did not exceed the TBLPF. As a result, sufficient SNR was only obtained at high frequencies and at the harmonics of the blade-rate frequency. As a result noise suppression by using near-field MVDR below 5 kHz did not result in an improvement and often lead to spurious results; we only present results of CSI. For acoustic noise the "advection velocity" in eq. (28) is the speed of sound and Corcos' correction does not apply above 5 kHz and above.

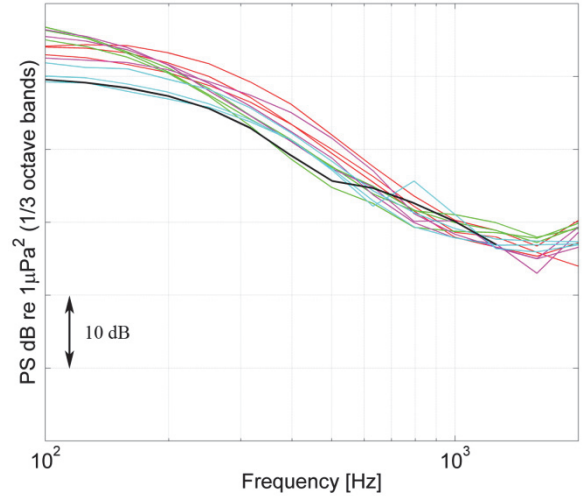


Figure 10: (Corrected) Goody's spectral estimate (black) compared to measurement data of several sensors in the array.

CAVITATION SOURCE LOCALISATION

For non-cavitating conditions, the coherence between sensors in a sub array was very low above the frequencies where TBLPF was present. An example of the coherence between two sensors for a cavitating condition is presented in Figure 11; for this particular case the ship sailed very slowly on the port-side shaft only with TBLPF present up to about 1-2kHz. From this figure a very clear trend was found in the phase behavior of the sensor pair.

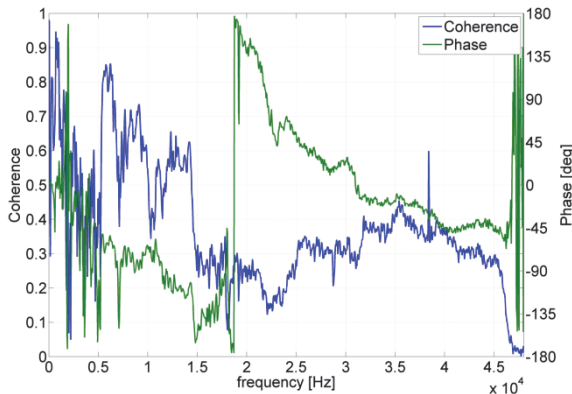


Figure 11: Coherence and wrapped phase between two sensors for a low ship speed running on one shaft only.

Interestingly, even when the coherence was low (<0.25) the source localization performed well provided the phase shift between sensors as function of frequency showed a clear trend; the value of the coherence by itself is apparently not a sufficient estimator of the quality of the measurement. The results of the individual sub arrays 1-3 as well as the combined IF is shown in Figure 12; each sub array individually operated as a far-field array as is apparent from the structure of the IFs and only the combined result indicates a location similar to the MS results in Figure 7C.

As the ship speed increased the coherence and trend in the phase between sensors slowly deteriorated; for the two most outboard sub arrays above 4 kHz both the amplitude coherence was poor and the coherent phase appeared to be random while the coherence and observable trend in the phase between transducers in the most inboard arrays remained very clear. When we calculate the streamlines running directly over the sub arrays by means of CFD (not presented), we observed that the streamlines for the outer sub arrays originated near the surface at the bow wave and for the inner sub arrays mid ship at some meters below the surface. Visualization of the propeller was hampered by bubbles so bubble sweep down from the bow wave may have influenced the propagation path

between the propeller and the transducers destroying the coherence and possibly generating noise of their own. As the conditions at low-speed with the single-shaft operation gave excellent coherence the authors hypothesize that bubble sweep down is the most plausible cause of the degradation in coherence for the more outboard sensors.

As the outer sub arrays were essentially lost for the array processing at higher speeds the array aperture was reduced, its ability to perceive depth deteriorated, and the IFs started to resemble a far-field solution. For normal, twin shaft operation, the incipient form of

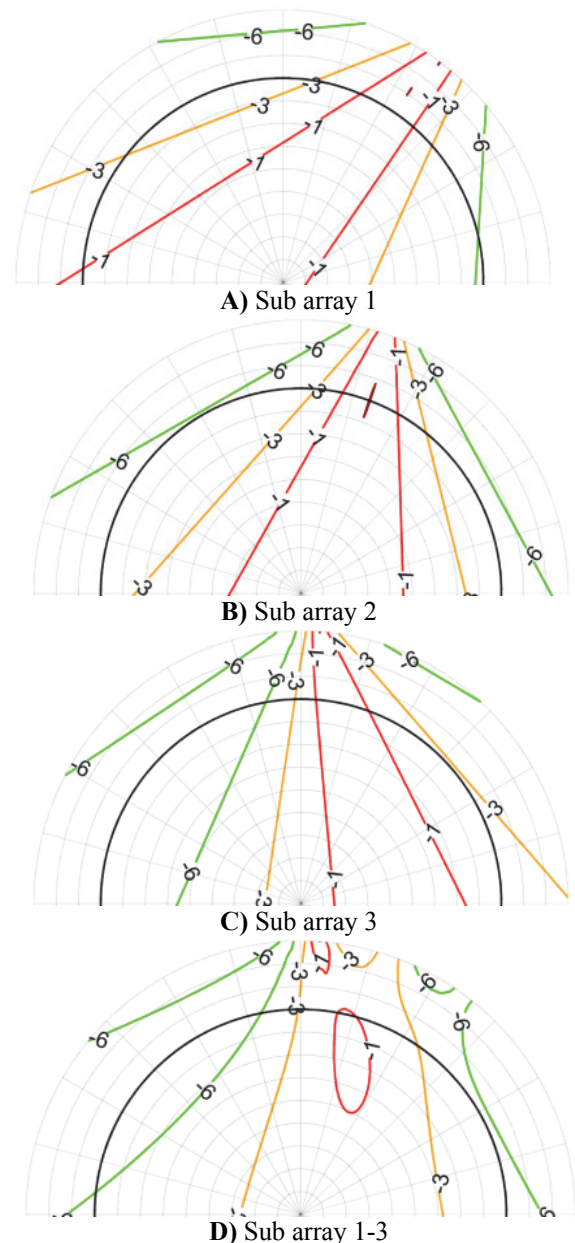


Figure 12: IFs at low speed, off design conditions, 10 kHz OTO band.

cavitation of this particular propeller was known to be suction-side sheet cavitation in the tip region on the downward going blade. The array processing estimated a source location near the edge of the search region *just outside* the propeller disc in the region of the downward going blade. The angular position of the localization estimation is considered to be in good agreement with expectations.

SOURCE LEVEL ESTIMATION

At higher speeds the array processing did not always return a plausible source location due to a lack of coherence between transducers in two of the most outward located sub arrays (S3 and S4). The radiated noise levels as measured by the transducers in sub array S1 consistently yielded the best SNR over the widest ship speed range. We therefore applied a source strength estimation using sub array S1 only assuming the same source location as for the single-shaft condition—corresponding to the cavitation location as observed during MS and FS tests for normal ahead sailing—and apply an empirical correction factor. The procedure is referred to here as the direct SL estimation. The mean noise levels at sensor were compared with the noise levels as registered by the beam aspect hydrophone (far field) of the noise range. Onboard measurements at lower speeds with an SNR < 5dB were not used. The onboard pressure levels were related to the noise range measurement, taking into account that a) for normal runs the onboard array only measures one of the two propellers, b) the solid boundary factor for the flush-mounted transducers is 2.0 c) the cavitating source is about 2 m removed from the transducers assuming spherical spreading loss and d) a correction to the contribution of the free surface image in the underwater noise levels (Lloyd’s mirror effect). We assumed a linear relation with unit slope between (corrected) onboard and far-field measurements and mean offsets were found to vary between -2 and +6 dB depending on the OTO band.

These mean offsets contain the effects of e.g., incorrect source location, influence of ship hull vibrations, cavitation noise sources outside the propeller disc, near-field effects of the source, and propagation effects different from spherical spreading loss. If we take these mean offsets as correction factors, we obtain the differences with the noise range measurement as given in Figure 13 for three ship speeds above the CIS. This procedure provides an estimate of the far-field noise using hull-mounted sensors with an accuracy of 3 dB.

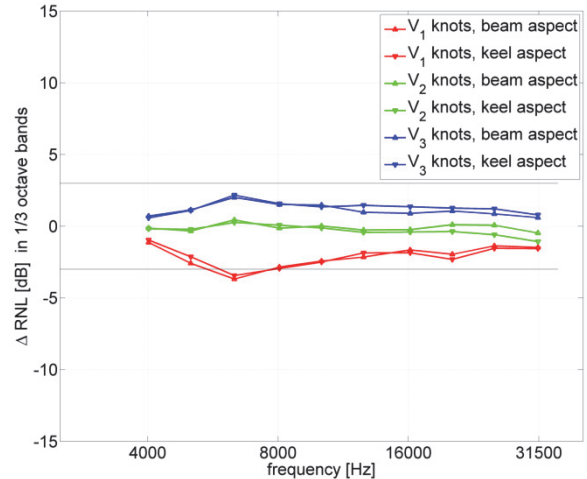


Figure 13: Differences between RNL of the direct estimation and far-field beam-aspect noise measurements (± 3 dB range indicated).

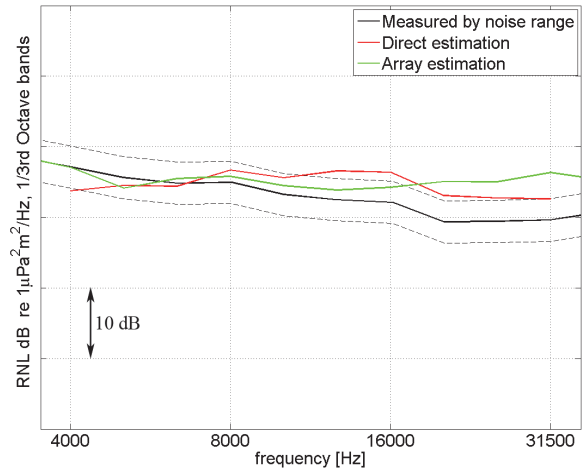


Figure 14: Comparison of the RNL estimation using the direct and the array method with the RNL measured by a beam-aspect hydrophone of the noise range (± 3 dB range indicated).

In Figure 14 results of the SL estimation from the single-shaft conditions at low ship speed are presented using the estimation from the array processing and the direct estimation using correction factors; this condition was not part of the runs used to derive the correction factors. The 3dB uncertainty lines represent the repeatability of the two pairs of measurements performed for the beam aspect hydrophone. The array estimation is accurate within 3 dB up to 16 kHz and the direct estimation is accurate to nearly 3dB over most of the frequency range. The main difference between the direct and array estimation is that the array estimation uses no calibration factors other than the assumed solid boundary factor of two.

The direct estimation was also tested for off-design conditions, whereby the ship sailed with unequal shaft loading—both pitch and rpm were unequal—at speeds where bubble sweep down prevented the array estimation from providing a reliable source location; two sets of measurements were performed; the portside and starboard side propeller settings were exchanged for the second set as no onboard array was fitted above the starboard propeller. The estimation from both runs were combined to provide an estimation for the ship noise and the estimation of the full scale noise measurements is within 3 dB of the noise range measurements for runs where suction-side cavitation was expected.

CONCLUSIONS

The use of an array of pressure transducers (PTs) for the estimation of the source level (SL) of far-field propeller cavitation noise and cavitation source localization has been successfully evaluated in model tests and full-scale trials. Near-field array processing techniques have been applied to localize the cavitation source in the propeller disc; Cross-Spectral Imaging (CSI) and Minimum Variation Distortionless Response (MVDR) in a near-field formulation. In both the model tests and full-scale trials the array processing was shown to give a plausible source location.

For model-scale verification tests using a sound emitter the location of the source could be very well located within 10% of the propeller diameter. The location of a sheet cavitation on the propeller in the model scale tests located well but with a large uncertainty; the signal-to-noise ratio (SNR) of the transducers is critical and needs to be improved.

For a flush-mounted PT the turbulent-boundary layer pressure fluctuations (TBLPF) may mask cavitation noise up to 1-5 kHz—depending on ship speed and the level of the cavitation noise—essentially prohibiting any array processing. The spectral content as measured correlated well with Goody's estimate

for TBLPF, corrected for the finite size of the transducer with the model as proposed by Corcos. As the noise from TBLPF is hydrodynamical and not acoustic, one option is to move the PTs away from the hull and mount them in shielded, acoustically transparent recesses. The use of a hydrophone protruding the hull located in the flow might be an option but self-noise and risk for debris impact must be managed.

At higher ship speeds the array coherence deteriorated rapidly for the more outboard PTs. It is hypothesized that bubbles—observed during the trials—presumably swept down from the bow are the cause. Tests of the array with the ship at lower speeds sailing on a single shaft only with an overloaded propeller showed excellent coherence and the array processing worked well.

The far-field cavitation noise was estimated using the array processing, and, a 'direct' method. The direct method used a fixed source location in combination with frequency-dependent correction factors varying between -2 and 6 dB, obtained from a number of speed runs on a noise range. With these correction factors a good prediction could be obtained not only for a range of ship speeds but also for off-design conditions. With the estimated source location from array processing no empirical correction was required to accurately estimate the far-field radiated noise.

Further research to the array application is required including other array layouts, processing techniques and noise-reduction algorithms, and, addressing the effect of bubble sweepdown. The effect of TBLPF is expected to be less important for ships with a low cavitation inception speed as the cavitation noise at moderate ship speeds can quickly become the dominating noise source, so that the presented method can provide a real-time estimate of the contribution of propeller cavitation noise during operational conditions without the need for noise-range calibration.

REFERENCES

- Abbot, P.A., Celuzza, S.A., Etter, R.J., "The acoustic characteristics of the naval surface warfare center's Large Cavitation Channel (LCC)", ASME Flow Noise Mod Meas Con., 1993, Vol. 168.
- Basten, T., de Jong, C., Graafland, F., van 't Hof, J., "Acoustic signature monitoring and management of naval platforms", 22nd Int Cong. Sound and Vibrations, July 2015, Florence, Italy.
- Bitzer, J. and Simmer, K.U., "Digital Signal Processing: Chapter 2: Superdirective Microphone arrays", ISBN 978-3-662-04619-7, Brandstein & Ward, editors.
- Bosschers, J, Lafeber, FH, de Boer, J, Bosman, R., and Bouvy, A., "Underwater Radiated Noise Measurements with a Silent Towing Carriage in the Depressurized Wave Basin", Adv Meas Tech Conf, Gdansk, Poland, 2013.
- Brandstein, M. and Ward, D, "Digital Signal Processing", 2001, ISBN 978-3-662-04619-7.
- de Bruijn, A., Moelker, W.H., and Absil, F.G.J. "Prediction method for the acoustic source strength of propeller cavitation", 2nd Int. Symp. on Shipboard Ac., , 1986, The Hague, Netherlands.
- Chang, N.A. and Dowling, D.R., Ray-based acoustic localization of cavitation in a highly reverberant environment, J. Ac. Soc. of Am., 2009, vol. 125 No. 5
- Christensen, J.J. and Hald, J., "Beamforming, Brüel & Kjaer Technical Review", 2004, No 1.
- Corcus, G.M., "Resolution of pressure in turbulence", J.Ac. Soc. of Am., 1963, vol 35(2), pp 192-199.
- Frost, O.L., "An algorithm for linearly constrained adaptive array processing", 1972, Proc. IEEE, vol 60(8), pp 926-935.
- Goody, M., , "Empirical spectral model of surface pressure fluctuations", AIAA Journal 2004, vol 42(9)
- Goody, M., Farabee, T., and Lee, Y.T., "Unsteady pressures on the surface of a ship hull", Int Mech Eng Congress Expo, November 11-15 2007 Seattle, Wa, USA.
- Kim, D., Seong, W., Choo, Y., and Lee, J., "Localization of incipient tip vortex cavitation using ray based matched field inversion method", J of Sound and Vibration, Vol. 354, 2015.
- Lafeber, F.H., Bosschers, J., de Jong, C., and Graafland, F., "Acoustic reverberation measurements in the Depressurized Wave Basin", Adv Meas Tech Conf, Istanbul, Turkey, 2015.
- Lafeber, F.H. and Bosschers, J., "Validation of computational and experimental prediction methods for the underwater radiated noise of a small research vessel", PRADS conf, Copenhagen, Denmark, 2016.
- Lee, J., Rhee, W., Ahn, B-K. , Choi, J-S., and Lee, C-S, 2012, Localization of singing noise on marine propellers using TDOA (Time Difference of Arrival) method. 29th Symp on Nav Hyd, August 2012, Gothenburg, Sweden.
- Lee, K., Lee, J., Kim, D., Kim, K., and Song, W., "Propeller sheet cavitation noise source modeling and inversion", J of Sound and Vibration Vol. 333, 2014.
- Newman, M., and Abrahamsen, K. "Measurement of underwater noise", Ship Noise and Vibration conf., 2007, London.
- Park, C., Seol, H., Kim, K., and Song, W., "A study on propeller noise source localization in a cavitation tunnel", Ocean Engineering, Vol. 36, 2009.
- Park, C., Kim, G-D., Park, Y-H., Lee, K., and Seong, W., "Noise localization method for model tests in a large cavitation tunnel using a hydrophone array", Remote Sensing, Vol. 8, 2016.
- Van der Kooij, J. and de Bruijn, A. "Acoustic Measurements in the NSMB Depressurized Towing Tank", Int Shipbuilding Progr Mar Tech Monthly, vol. 31(353), 1984.
- van Terwisga, T.J.C., Noble, D.J., Veer, R, van 't, Assenberg, F., McNeice, B., and Terwisga, P.F., van, "Effect of operational conditions on the cavitation inception speed of naval propellers", 25th symp. on Nav. Hyd., 2004, St Johns, Canada.
- van Wijngaarden, H.C.J., "Prediction of propeller-induced hull-pressure fluctuations", PhD thesis, 2011, Delft University of Technology.
- ten Wolde, T., and de Bruijn, A., "A new method for the measurement of the acoustical source strength of cavitating ship propellers", Int Shipbuilding Pro. 1975, Vol. 22(255).